Monthly Notices
of the
ROYAL ASTRONOMICAL SOCIETY

MNRAS **485,** 1460–1476 (2019)
Advance Access publication 2019 February 19

doi:10.1093/mnras/stz505

The eye of *Gaia* on globular clusters kinematics: internal rotation

A. Sollima [1]★ H. Baumgardt [2] and M. Hilker[3]

[1]*INAF Osservatorio di Astrofisica e Scienza dello spazio di Bologna, via Gobetti 93/3, I-40129 Bologna, Italy*
[2]*School of Mathematics and Physics, The University of Queensland, St Lucia, QLD 4072, Australia*
[3]*European Southern Observatory, Karl-Schwarzschild-Str 2, D-85748 Garching, Germany*

Accepted 2019 February 15. Received 2019 February 11; in original form 2018 October 25

ABSTRACT

We derived the three-dimensional velocities of individual stars in a sample of 62 Galactic globular clusters using proper motions from the second data release of the *Gaia* mission together with the most comprehensive set of line-of-sight velocities with the aim of investigating the rotation pattern of these stellar systems. We detect the unambiguous signal of rotation in 15 clusters at amplitudes which are well above the level of random and systematic errors. For these clusters, we derived the position and inclination angle of the rotation axis with respect to the line of sight and the overall contribution of rotation to the total kinetic energy budget. The rotation strengths are weakly correlated with the half-mass radius, the relaxation time, and anticorrelated with the destruction rate, while no significant alignment of the rotation axes with the orbital poles has been observed. This evidence points towards a primordial origin of the systemic rotation in these stellar systems.

Key words: methods: data analysis – methods: statistical – techniques: radial velocities – proper motions – stars: kinematics and dynamics – globular clusters: general.

1 INTRODUCTION

Among old (>10 Gyr) stellar systems, globular clusters (GCs) are those with the largest ratio between age and half-mass relaxation time. A typical GC star completed hundreds of orbits within the cluster potential and the chance of interaction with another star, which changes its orbit, is significant. The effect of a large number of interactions is to randomize the directions of individual orbits and to lead towards a velocity distribution tending to a Maxwellian-like distribution. For this reason, GCs are the prototype of pressure-supported stellar system, in which the gravitational potential energy of the cluster is balanced by the kinetic energy residing in random motions. On the basis of the above considerations, the kinematics of GCs has been widely investigated through the comparison with isotropic non-rotating models (like e.g. King 1966, models) in a large number of past studies (McLaughlin & van der Marel 2005; Baumgardt 2017; Hénault-Brunet et al. 2019, and references therein).

Nevertheless, deviations from isotropy can be present in the velocity distribution of GC stars in the form of ordered motions (i.e. rotation) and/or preferential orientation of the velocity ellipsoid (i.e. anisotropy). Neglecting such effects can affect the determination of dynamical parameters of GCs like e.g. their masses (Sollima et al. 2015). In particular, the presence of rotation has deep relevance for the equilibrium of these stellar systems contributing to their kinetic energy budget and possibly leading to a flattening of their shape in the direction parallel to the rotation axis (Wilson 1975).

Rotation in GCs can either be relic of the initial conditions of these objects at the epoch of their formation or originate from the interaction with the Galactic tidal field within which they move (Keenan & Innanen 1975; Mapelli 2017). Although the formation mechanism of GCs is still not completely understood, a possible picture of their birth environment is provided by theoretical simulations of star-forming complexes. In these environments turbulence-supported molecular clouds possess several clumps which merge over a time-scale of a few Myr (Mapelli 2017). The large-scale torques occurring during the hierarchical assembly of these clumps imprint a significant rotation to the embedded cluster which is enhanced during its early collapse because of angular momentum conservation. During the subsequent long-term evolution, two-body relaxation tends to erase such a rotation pattern. The dampening of the rotation signal is additionally caused by the ever-continuing mass-loss experienced by the cluster which carry away angular momentum (Tiongco, Vesperini & Varri 2017). Part of the original rotation can however survive till the present day and be observable in the velocity distribution of GC stars. A certain degree of rotation can also develop in the cluster outskirts because of tidal effects. Indeed, at large distance from the cluster centre Coriolis force is directed inward/outward according to the direction of the stellar motion with respect to the systemic cluster orbit, with stars on prograde orbits more easily expelled by the cluster (Henon 1970;

★ E-mail: antonio.sollima@inaf.it

Vesperini et al. 2014). On the long term this effect produces a low-amplitude retrograde rotation whose axis is aligned with the cluster orbital pole and with a period synchronized with the cluster orbital period (Tiongco, Vesperini & Varri 2016, 2018). The measure of rotation in a statistically meaningful sample of GCs is therefore crucial to study the efficiency and frequency of the above processes.

The main effect of rotation is a shift in the mean tangential motion along a preferential axis. Such a shift reflects in the velocity distribution along all the three components in proportions depending on the position angle and the inclination with respect to the line of sight of the rotation axis. Thus, a thorough analysis of rotation requires an estimate of all three velocity components. The lack of accurate proper motions has represented a major issue in the analysis of rotation of GCs till recent years. For this reason, the large majority of the studies conducted in the past on this topic were performed for GCs which are under favourable projection conditions (i.e. in case of edge-on rotation), where rotation leaves a detectable sinusoidal modulation of the mean line-of-sight velocity as a function of the azimuthal position of the stars (see Section 3.3). The most recent and comprehensive studies based on large samples of line-of-sight velocities analysed a few tens of GCs (Lane et al. 2010; Bellazzini et al. 2012; Fabricius et al. 2014; Kimmig et al. 2015; Lardo et al. 2015; Ferraro et al. 2018; Kamann et al. 2018). In these studies, only the rotation velocity projected along the line of sight was determined and no information on the actual inclination of the rotation axis could be derived. In spite of this limitation, these studies revealed correlations between the rotation strength and various general (horizontal branch morphology, absolute magnitude, metallicity; Bellazzini et al. 2012; Lardo et al. 2015), structural (e.g. ellipticity; Fabricius et al. 2014), and dynamical (half-mass relaxation time; Kamann et al. 2018) parameters. On the other hand, recent studies based on the analysis of proper motions measured have been conducted for the most massive and nearby clusters ω Centauri (van Leeuwen et al. 2000; van de Ven et al. 2006; Libralato et al. 2018) and 47 Tucanae (Anderson & King 2003; Bellini et al. 2017) and NGC 6681 (Massari et al. 2013).

A revolution in this field is provided by the astrometric mission *Gaia* which measures parallaxes and proper motions for $\sim 10^9$ stars in both hemispheres with accuracies <30 μas (corresponding to $<1.5\,\mathrm{km\,s^{-1}}$ at a distance of 10 kpc) sampling also thousands of stars in the outer regions of all Galactic GCs (Gaia Collaboration 2018a). In a recent paper, Bianchini et al. (2018) used the data from the *Gaia* second data release to investigate rotation in a sample of 51 GCs and detected a 3σ significant evidence in 11 of them. For a subsample of eight GCs with available line-of-sight velocities they also provide an estimate of the inclination angle of the rotation axis with respect to the line of sight. This last work constitutes the most extensive survey for rotation in Galactic GCs in terms of accuracy and completeness to date. They confirm the correlation between the relevance of rotation over random motions and the half-mass relaxation time. On the other hand, their work is based on proper motions only, thus suffering a similar detection bias of studies based on line-of-sight velocities only. In particular, while their analysis has an excellent sensitivity in detecting rotation in the plane of the sky, a rotation along the line of sight would not leave any significant signal in the proper motions domain. Moreover, the presence of covariances and small-scale systematics in the *Gaia* proper motions (Arenou et al. 2018) enhance the chance of false detections. Finally, the lack of line-of-sight velocity information does not allow to derive the actual rotational velocity and inclination of the rotation axis for all the GCs of their sample.

In this paper we correlate the proper motions from the *Gaia* second data release with the most extensive survey of line-of-sight velocities collected by Baumgardt & Hilker (2018). This allows to derive 3D velocities for more than 42 000 stars in 62 Galactic GCs which are used to search for any significant rotation signal among these stellar systems. We introduce the observational material and the sample selection in Section 2. The method adopted to detect rotation in our sample is described in Section 3. Section 4 is devoted to the modelling of the observed kinematics of GCs with a significant signal of rotation. We analyse correlations with various general and dynamical parameters in Section 5. Finally, we discuss and summarize our results in Section 6.

2 OBSERVATIONAL MATERIAL

The analysis performed in this paper is based on two main data bases: (i) the sample of line-of-sight velocities collected by Baumgardt & Hilker (2018), and (ii) the proper motions of the *Gaia* second data release (Gaia Collaboration 2018a). The line-of-sight velocity sample consists of 45 561 velocities measured in 109 Galactic GCs. It is a compilation of homogeneous measures from spectra obtained at the Very Large Telescope of the European Southern Observatory and Keck telescope with different instruments, which are complemented by published line-of-sight velocities in the literature. A detailed description of the sample selection, reduction, and data analysis process as well as the complete list of references for the data resources is provided in Baumgardt & Hilker (2018) and Baumgardt et al. (2019). The sample covers a wide portion of the clusters' extent with a median uncertainty of $0.5\,\mathrm{km\,s^{-1}}$.

For each target cluster we extracted from the *Gaia* public archive[1] the proper motions of all stars within the tidal radius (from McLaughlin & van der Marel 2005). We do not apply any selection on either the *Gaia* quality flag, parallaxes, or colour–magnitude diagram. Indeed, we found that any selection made on these basis provides only a marginal improvement in terms of accuracy and purity against fore/background contaminants while significantly reducing the sample size (see Section 3.2). Proper motions (μ_{RA} cosDec., $\mu_{\mathrm{Dec.}}$) and their corresponding uncertainties have been converted into velocities (v_{RA}, $v_{\mathrm{Dec.}}$) using equation 2 of Gaia Collaboration (2018b) assuming the distance listed in the Harris (1996, 2010 edition) catalogue and corrected for perspective rotation using equations 4 and 6 of van de Ven et al. (2006).

The two above samples have been cross-correlated providing 3D velocities for a subsample of stars in each cluster. The celestial coordinates (RA, Dec.) have been converted into projected distances from the cluster centre (X,Y) using equation 1 of van de Ven et al. (2006) and adopting the centres of Goldsbury, Heyl & Richer (2013).[2] The systemic motion of each cluster ($\langle v_{\mathrm{LOS}}\rangle$, $\langle v_{\mathrm{RA}}\rangle$, $\langle v_{\mathrm{Dec.}}\rangle$) has been determined by maximizing the likelihood

$$lnL = -\frac{1}{2}\sum_i \left[\frac{(v_{\mathrm{LOS},i} - \langle v_{\mathrm{LOS}}\rangle)^2}{s^2_{\mathrm{LOS},i}} + ln(s^2_{\mathrm{LOS},i}(1-\tilde{\rho_i}^2)) + \sum_{j=\mathrm{RA,Dec.}} \left(\frac{(v_{j,i} - \langle v_j\rangle)^2}{(1-\tilde{\rho_i}^2)s^2_{j,i}} + ln(s^2_{j,i}) \right) - \frac{2\tilde{\rho_i}(v_{\mathrm{RA},i} - \langle v_{\mathrm{RA}}\rangle)(v_{\mathrm{Dec.},i} - \langle v_{\mathrm{Dec.}}\rangle)}{(1-\tilde{\rho_i}^2)s_{\mathrm{RA},i}s_{\mathrm{Dec.},i}} \right], \quad (1)$$

[1] http://gea.esac.esa.int/archive/.

[2] For those clusters not included in the Goldsbury et al. (2013) sample, we adopted the centres listed in the Harris (1996, 2010 edition) catalogue.

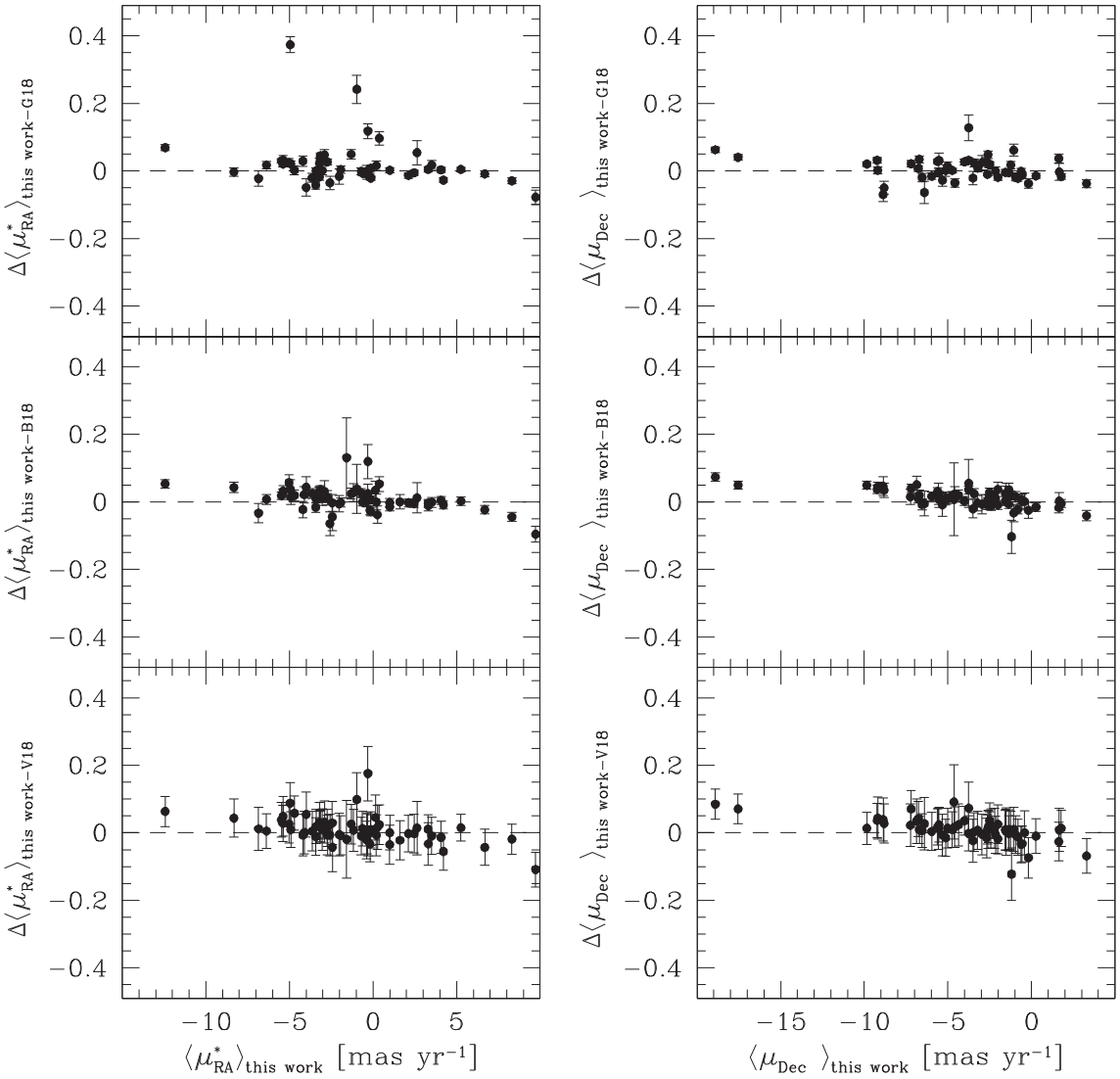

Figure 1. Comparison between the systemic proper motions estimated by Gaia Collaboration (2018b, top panels), Baumgardt et al. (2019, middle panels), Vasiliev (2019, bottom panels), and this work. The dashed line marks the one-to-one relation in all panels.

where

$$s^2_{j,i} = \sigma^2_{j,i} + \epsilon^2_{j,i} \qquad j = \text{LOS, RA, Dec.}$$
$$\tilde{\rho}_i = \rho_i \frac{\epsilon_{\rm RA}\epsilon_{\rm Dec.}}{s_{\rm RA}s_{\rm Dec.}}$$

In the above equation $\sigma_{j,i}$ and $\epsilon_{j,i}$ are the velocity dispersion and error of the i-th star in the j-th component (either LOS, RA, or Dec.) and ρ_i is the covariance between $v_{\rm RA}$ and $v_{\rm Dec}$. We neglected the covariances involving RA and Dec. (because of their negligible amplitudes) and those involving parallax (since this parameter does not enter in equation 1 and its uncertainty is therefore marginalized over the other parameters).

The intrinsic velocity dispersion in any one direction at the projected distance of each star from the cluster centre ($\sigma_{j,i} \equiv \sigma(R_i)$; assumed the same in all the three components) has been calculated by multiplying the amplitude of the line-of-sight velocity dispersion profile of the best-fitting King (1966) model provided by McLaughlin & van der Marel (2005) by the normalization factor providing the best fit to observational data. We decided to normalize the amplitude of the velocity dispersion profile using only line-of-sight velocities since proper motions have systematically larger dispersions. This possibly arises from either an underestimate of the reported uncertainty or the possible presence of small-scale systematics (see also Section 3.2).

An iterative algorithm has been employed to calculate the mean velocities by excluding at each iteration stars with

$$\sum_j \left(\frac{(v_{j,i} - \langle v_j\rangle)}{s_j}\right)^2 > 25$$

and renormalizing the σ profile on the sample of retained stars. The above algorithm generally converges after a few iterations providing the systemic velocity along the three components, the amplitude of the intrinsic velocity dispersion profile, and a sample of bona fide cluster members. In Fig. 1 the estimated systemic proper motions are compared with the results by Gaia Collaboration (2018b), Baumgardt et al. (2019), and Vasiliev (2019). We find an excellent agreement between our estimates and those provided by these works.

The sizes of the final samples range from 10 to ∼2500 stars according to the cluster distance and mass. Among the whole set of 109 GCs we selected only those 62 GCs with at least 50 member stars with measurements in all the three velocity components. We used these samples to search for rotation signals as described in Section 3. For those clusters with positive detections, in Section 4 we fit dynamical models to extended samples containing all stars with *at least* one measured velocity component and within $3s_{j,i}$ from the systemic velocity.

In the following sections we will refer to a system of coordinates in space (*X*,*Y*,*Z*) and velocity (v_X, v_Y, v_Z) where the coordinates of the cluster centre and the systemic cluster motion have been subtracted

$$v_X = v_{\rm RA} - \langle v_{\rm RA}\rangle$$
$$v_Y = v_{\rm Dec.} - \langle v_{\rm Dec.}\rangle$$
$$v_Z = v_{\rm LOS} - \langle v_{\rm LOS}\rangle\,.$$

3 METHOD

3.1 Algorithm

The effect of rotation can be detected as a modulation of the mean velocity as a function of the position angle. In particular, for a solid-body rotation with angular velocity ω the mean velocity in the three components is

$$\begin{aligned} v_Z &= \omega\ R\ \sin(\theta-\theta_0)\sin i \\ v_\parallel &= \omega\ R\ \sin(\theta-\theta_0)\cos i \\ v_\perp &= \omega\ [R\ \cos(\theta-\theta_0)\cos i + Z\sin i]\,, \end{aligned} \qquad (2)$$

where R is the projected distance from the cluster centre, i is the inclination angle of the rotation axis with respect to the line of sight, θ is the position angle (defined anticlockwise from the *Y*-axis), θ_0 is the position angle of the rotation axis, $v_{\parallel}$ and $v_\perp$ are the velocity components in the directions parallel and perpendicular to the rotation axis, respectively (see Appendix A).

In a real cluster the angular velocity ω is a function of the distance from the rotation axis. In particular, past studies found that rotating stellar systems show a solid-body rotation in their innermost region with an increasing mean rotational velocity till a projected distance where the rotation amplitude reaches a maximum ($\omega \sim$ *constant* at $R < R_{\rm peak}$) and then declines monotonically at larger distances (Wilson 1975). To account for this effect in a rigorous way a rotating model should be fitted to the data. However, this would introduce a dependence of the detection efficiency on the assumptions of the adopted model. To perform a model-independent analysis we considered an average projected rotation velocity $A = \langle\omega\ R\rangle$ amplitude which has been assumed to be independent on distance. Note that this approximation does not introduce any bias in the estimate of the position angle and inclination of the rotation axis since these quantities are calculated from the ratio of amplitudes in v_Z, $v_{\parallel}$, and $v_\perp$ and the term $\omega\ R$ appears as a multiplicative factor in all the three equation 2. So, as long as the same stars are used to compute the mean amplitudes in the three components, any change in the $\omega\ R$ factor of individual stars erases when relative amplitudes are computed.

In principle, the first two equations of 2 allow to determine the values of θ_0, i, and A. However, part of the information is lost in neglecting the third equation which can increase the detection efficiency while reducing the chance of false detections. The third equation is complicated due to the presence of the unknown distance along the line of sight (Z) as an independent variable. The dependence on Z does not affect the mean trend of $v_\perp$ (since $\langle Z\rangle = 0$) but introduces an additional spread in $v_\perp$ equal to $\sigma_{\perp,Z} = \sigma_Z A\ \sin i/R$, where σ_Z is the spread in Z as a function of the projected distance R. Although $\sigma_{\perp,Z}$ can be calculated from the cluster density profile and the first two equations of 2, we decided to neglect this spread. Indeed, the term σ_Z/R is negligible outside the innermost cluster region. On the other hand, at such a small distance the assumption of constant A is no more reliable and in real clusters we expect $A \propto R$ implying small values of $\sigma_{\perp,Z}$ also in this region.

For each cluster of our sample we searched for the values of θ_0, i, and A which maximize the likelihood

$$\begin{aligned} lnL = -\frac{1}{2}\sum_i \Bigg[& \frac{(v_{Z,i}-\overline{v_{Z,i}})^2}{s^2_{Z,i}} + ln(s^2_{{\rm LOS},i}(1-\overline{\rho_i}^2)) \\ & + \sum_{j=\parallel,\perp}\left(\frac{(v_{j,i}-\overline{v_j})^2}{(1-\overline{\rho_i}^2)s^2_{j,i}} + ln(s^2_{j,i})\right) \\ & - \frac{2\overline{\rho_i}(v_{\parallel,i}-\overline{v_{\parallel,i}})(v_{\perp,i}-\overline{v_{\perp,i}})}{(1-\overline{\rho_i}^2)s_{\parallel,i}s_{\perp,i}}\Bigg] \end{aligned} \qquad (3)$$

where

$$s^2_{j,i} = \sigma^2_{j,i} + \epsilon^2_{j,i} \qquad j = {\rm LOS},\parallel,\perp$$
$$\epsilon^2_{\parallel,i} = \epsilon^2_{{\rm RA},i}\sin^2\theta_0 + \epsilon^2_{{\rm Dec.},i}\cos^2\theta_0 - 2\rho_i\epsilon_{{\rm RA},i}\epsilon_{{\rm Dec.},i}\sin\theta_0\cos\theta_0$$
$$\epsilon^2_{\perp,i} = \epsilon^2_{{\rm RA},i}\cos^2\theta_0 + \epsilon^2_{{\rm Dec.},i}\sin^2\theta_0 + 2\rho_i\epsilon_{{\rm RA},i}\epsilon_{{\rm Dec.},i}\sin\theta_0\cos\theta_0$$
$$\overline{\rho_i} = \frac{1}{s_{\parallel,i}s_{\perp,i}}\left[\frac{(\epsilon^2_{{\rm Dec.},i}-\epsilon^2_{{\rm RA},i})}{2}\sin2\theta_0 + \rho_i\epsilon_{{\rm RA},i}\epsilon_{{\rm Dec.},i}\cos2\theta_0\right]$$
$$\overline{v_{Z,i}} = A\ \sin(\theta_i-\theta_0)\sin i$$
$$\overline{v_{\parallel,i}} = A\ \sin(\theta_i-\theta_0)\cos i$$
$$\overline{v_{\perp,i}} = A\ \cos(\theta_i-\theta_0)\cos i$$

In the above notation $0^\circ < i < 90^\circ$ is defined with respect to the line of sight, $0^\circ < \theta_0 < 360^\circ$ grows anticlockwise from North to West and A is positive for clockwise rotation in the plane of the sky.

The above algorithm returns best-fitting values of θ_0, i, and A for all the 62 GCs of our sample. An example of best fit of the velocity distribution in the three components is shown in Fig. 2 for NGC 104.

To evaluate the significance of rotation we employed a Monte Carlo technique: for each cluster, 10^4 mock observations of a non-rotating system have been simulated by randomly extracting velocities in the three components from Gaussian functions centred at v_Z, $v_{\rm RA}$, $v_{\rm Dec.} = 0$ and with dispersion equal to the local velocity dispersion σ_i at the position of the real stars. The measurement errors have been then added as Gaussian shift with amplitude equal to the observational uncertainties of real stars (including covariances between $v_{\rm RA}$ and $v_{\rm Dec.}$) and the best-fitting value of the rotation amplitude has been calculated using the same technique adopted for real data. The fraction of simulations with best-fitting amplitudes smaller than the one obtained on real data gives the probability that the observed rotation signal is not produced by fluctuations. An additional set of Monte Carlo simulations has been run for the clusters with positive detection of rotation assuming the position-dependent velocity shift in the three velocity components predicted by the best-fitting models (see Section 4). The standard deviations of the derived parameters (i, θ_0, A, ξ) have been assumed as the

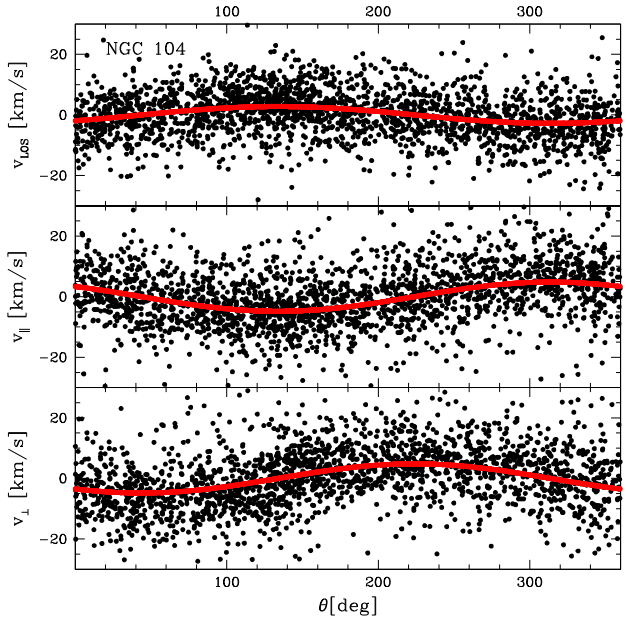

Figure 2. Distribution of the three velocity components as a function of the position angle for NGC 104 (the entire set of best fits for the 15 GCs with positive detection of rotation is available in the online version of the paper). The position angle is defined from North to West (see Section 3.1). The red solid lines show the best-fitting trend in all panels.

corresponding uncertainties. They do not include the uncertainty on the adopted cluster heliocentric distance, which affects both the rotation amplitude and the inclination angle as a systematic error in the following way

$$A = \sqrt{A_{\rm LOS}^2 + A_{\mu}^2 {\rm d}^2}$$

$$i = \tan^{-1}\left(\frac{A_{\rm LOS}}{A_{\mu}{\rm d}}\right)$$

where $A_{\rm LOS}$ and A_{μ} are the amplitude measured in the line-of-sight velocity and proper motion spaces, respectively.

We list the best-fitting amplitudes and the corresponding rotation probabilities for the entire set of 62 GCs of our sample in Table 1.

3.2 Effect of sample selection, random, and systematic errors in *Gaia* proper motions

We find a rotation signal at $>3\sigma$ significance level in 24 GCs (see Table 1). However, as stated in Section 2, we found that the intrinsic dispersion of proper motions is systematically larger than that of line-of-sight velocities. This effect can indicate an underestimate of the uncertainties of proper motions, the presence of small-scale systematics or by a significant contamination from Galactic interlopers. In the following we will check if these effects can produce false detections in our sample.

In principle, random fluctuations increase the spread of the velocity distribution without affecting the mean trend produced by rotation. However, an underestimate of random errors affects the results of the Monte Carlo technique spuriously increasing the significance level of the rotation signal. To quantify such an effect, we run the Monte Carlo simulations for the GCs with positive detection multiplying the proper motion errors by the fudge factor required to match the intrinsic dispersion of line-of-sight velocities. With this approach we confirm a significant rotation signal in 23 out of 24 GCs, with only NGC 5824 being excluded from the sample.

A more subtle effect can be produced by systematic errors. It is indeed known that the inhomogeneous sampling of *Gaia* is responsible for the presence of systematic shifts in proper motions. These errors have amplitudes $\mu < 0.07\,{\rm mas\,yr^{-1}}$ and follow a patchy structure with both small- and large-scale variations (Lindegren et al. 2018). The presence of an inhomogeneous distribution of proper motions within the cluster field of view can produce an azimuthal variation mimicking a spurious rotation in the plane of the sky. Actually, if we convert the rotation velocity component on the plane of the sky into proper motion we find that 19 GCs among those with positive detections have amplitudes $<0.1\,{\rm mas\,yr^{-1}}$, with the exception of NGC 104, NGC 5139, NGC 6266, and Ter 5. However, to produce a spurious rotation signal, the amplitude of proper motion systematics must be accompanied by a negligible amplitude in line-of-sight velocity at the same position angle. To test this effect, we calculate rotation amplitudes in our Monte Carlo simulations only from line-of-sight velocities and fixing the position and inclination angles of the rotation axis to those measured in real clusters. In this case, only 15 GCs maintain a significant rotation signal. They are listed in Table 2 together with their best-fitting rotation amplitudes, position, and inclination angles. For the eight GCs excluded by this last criterion (namely, NGC 1904, NGC 5272, NGC 6093, NGC 6218, NGC 6341, NGC 6752, NGC 6809, and NGC 7099; hereafter referred as 'uncertain') we cannot exclude the presence of a genuine rotation mainly in the plane of the sky with amplitudes below the typical level of *Gaia* systematics. Nevertheless, in the following sections we will conservatively consider only the 15 GCs with an unambiguous evidence of rotation.

Another possible source of missing/false detection could be in principle due to the contamination from Galactic field stars or astrometric artefacts. Velocity gradients in the fore/background Galactic component surrounding our analysed GCs are indeed present and can potentially produce a spurious rotation signal. However, the 3D velocity selection criteria described in Section 3.1 are extremely effective in selecting a genuine sample of bright member stars: a comparison with the Robin et al. (2003) Galactic model predicts a contamination < 0.2 per cent in all the GCs of our sample with the exception of those GCs immersed in the bulge for which a few per cent contamination is possible close to their tidal radii, where only a few stars are sampled. Moreover, over the relatively small extent of our GCs (< 1 deg for the most extended GCs in the halo and <0.3 deg for bulge GCs), the Galactic rotation pattern translates into a non-negligible signal only along the Galactic bar.

Astrometric artefacts can also increase the noise in the v–θ plane thus reducing the detection efficiency. Consider however that the detection efficiency is only marginally dependent on errors. This is because the rotation signal depends on the amplitude of the mean velocity. So, by including stars with a large (or slightly underestimated) error would increase the spread around the mean trend without affecting the amplitude.

As stated in Section 2 we have not applied any selection criteria based on neither *Gaia* quality flags nor on the distance from the cluster centre. To test the effect of more strict member selection on our results, we also performed the analysis adopting two different selection criteria: (i) we exclude stars outside half of the nominal tidal radius (from McLaughlin & van der Marel 2005) and those with a proper motion error exceeding 1.5 times the central velocity dispersion, and (ii) select only stars included in the member list provided by Gaia Collaboration (2018b). In both cases, we confirm

Table 1. Results for all the analysed GCs. The classes are assigned to GCs in any of the following categories: r: rotating ($P > 99.7$ per cent and satisfying all the performed tests), u: uncertain ($P > 99.7$ per cent but fails one of the tests against random/systematic uncertainties; see Section 3.2).

Name	A km s^{-1}	P per cent	Class	Name	A km s^{-1}	P per cent	Class	Name	A km s^{-1}	P per cent	Class
Arp 2	4.06 ± 4.15	67.6		NGC 5904	4.11 ± 0.42	100.0	r	NGC 6522	1.43 ± 2.21	24.4	
NGC 104	5.00 ± 0.32	100.0	r	NGC 5927	0.93 ± 0.72	82.2		NGC 6539	1.94 ± 1.15	95.9	
NGC 288	0.42 ± 0.32	84.3		NGC 5986	1.65 ± 0.93	97.7		NGC 6541	3.73 ± 1.15	100.0	r
NGC 362	0.51 ± 0.56	53.0		NGC 6093	1.97 ± 0.84	99.7	u	NGC 6553	2.33 ± 0.82	100.0	r
NGC 1261	0.90 ± 0.64	86.9		NGC 6121	0.22 ± 0.17	81.8		NGC 6569	0.81 ± 0.91	52.3	
NGC 1851	0.45 ± 0.42	71.2		NGC 6171	0.70 ± 0.46	93.9		NGC 6624	0.87 ± 1.04	46.7	
NGC 1904	2.24 ± 0.46	100.0	u	NGC 6205	1.53 ± 0.61	99.9	r	NGC 6626	2.42 ± 1.08	100.0	r
NGC 2808	2.25 ± 0.56	100.0	r	NGC 6218	0.93 ± 0.37	100.0	u	NGC 6656	3.38 ± 0.71	100.0	r
NGC 3201	0.80 ± 0.41	98.8		NGC 6254	0.26 ± 0.56	12.0		NGC 6712	0.58 ± 0.69	45.8	
NGC 4372	1.36 ± 0.68	99.2		NGC 6266	6.22 ± 1.53	100.0	r	NGC 6715	0.57 ± 1.11	18.5	
NGC 4590	0.27 ± 0.51	17.2		NGC 6273	4.19 ± 1.12	100.0	r	NGC 6723	0.84 ± 0.55	93.0	
NGC 4833	1.14 ± 0.83	86.6		NGC 6304	1.30 ± 0.91	89.4		NGC 6752	0.91 ± 0.34	99.9	u
NGC 5024	1.17 ± 0.62	99.5		NGC 6341	1.46 ± 0.61	99.9	u	NGC 6779	1.09 ± 1.52	35.1	
NGC 5053	0.36 ± 0.90	15.5		NGC 6362	0.47 ± 0.40	75.2		NGC 6809	0.88 ± 0.38	99.9	u
NGC 5139	4.27 ± 0.52	100.0	r	NGC 6366	0.63 ± 0.60	66.6		NGC 6838	0.74 ± 0.42	97.8	
NGC 5272	1.75 ± 0.42	100.0	u	NGC 6388	1.51 ± 0.65	99.5		NGC 7078	3.29 ± 0.51	100.0	r
NGC 5286	0.76 ± 0.95	40.6		NGC 6397	0.48 ± 0.17	100.0	r	NGC 7089	3.01 ± 0.70	100.0	r
NGC 5466	0.84 ± 0.65	81.3		NGC 6402	1.58 ± 0.88	97.7		NGC 7099	1.10 ± 0.40	100.0	u
NGC 5694	5.62 ± 6.40	62.3		NGC 6440	3.93 ± 2.74	87.5		Terzan 5	7.97 ± 2.38	100.0	r
NGC 5824	6.47 ± 2.28	99.7	u	NGC 6441	1.52 ± 1.66	55.3		Terzan 8	0.79 ± 1.51	37.5	
NGC 5897	1.02 ± 0.79	82.0		NGC 6496	1.21 ± 0.63	97.1					

Table 2. List of rotating GCs.

Name	A km s^{-1}	θ_0 deg	i deg	ξ
NGC 104	-5.00 ± 0.32	224.3 ± 4.6	33.6 ± 1.8	0.102 ± 0.003
NGC 2808	-2.25 ± 0.56	36.1 ± 8.4	88.5 ± 10.3	0.020 ± 0.005
NGC 5139	4.27 ± 0.52	170.2 ± 7.6	39.2 ± 4.4	0.045 ± 0.002
NGC 5904	4.11 ± 0.42	221.6 ± 6.0	42.6 ± 3.2	0.137 ± 0.011
NGC 6205	-1.53 ± 0.61	165.5 ± 14.2	85.9 ± 11.6	0.131 ± 0.032
NGC 6266	6.22 ± 1.53	104.2 ± 46.1	15.0 ± 12.8	0.043 ± 0.006
NGC 6273	4.19 ± 1.12	56.9 ± 13.2	41.9 ± 7.1	0.065 ± 0.010
NGC 6397	-0.48 ± 0.17	8.6 ± 15.6	72.8 ± 11.9	0.004 ± 0.001
NGC 6541	-3.73 ± 1.15	83.2 ± 18.3	65.4 ± 13.9	0.083 ± 0.027
NGC 6553	2.33 ± 0.82	237.7 ± 38.4	75.6 ± 29.5	0.003 ± 0.007
NGC 6626	-2.42 ± 1.08	28.6 ± 17.7	83.5 ± 13.3	0.018 ± 0.011
NGC 6656	3.38 ± 0.71	252.8 ± 9.2	62.1 ± 6.3	0.091 ± 0.008
NGC 7078	3.29 ± 0.51	52.6 ± 28.8	15.4 ± 5.4	0.071 ± 0.009
NGC 7089	-3.01 ± 0.70	346.6 ± 12.1	52.9 ± 11.2	0.071 ± 0.015
Terzan 5	7.97 ± 2.38	260.4 ± 48.5	26.9 ± 34.6	0.026 ± 0.007

the significant rotation in the same 15 GCs. Regarding the selection criterion (i), we also confirm the uncertain signal in eight out of nine GCs listed in Table 1, with the exception of NGC 5824 for which the number of member stars reduces below the threshold set at 50 objects. As already noticed in Baumgardt et al. (2019), the application of a proper motion error selection criterion improves the agreement between the dispersion measured along the line-of-sight and the transverse directions. The estimated inclination angles and rotation strengths agree within the combined uncertainties with those measured in the unselected sample, although in the selected sample the uncertainties are larger because of the reduced sample sizes. The application of the selection criterion (ii) excludes from our sample a small fraction <2 per cent in all the analysed GCs with no significant effect in the resulting detection as well as in the estimated inclination angles and rotation strengths.

On the basis of the above test we conclude that, for the purpose of this work, quality and radial selection criteria do not affect the detection efficiency while reducing the accuracy of the estimated quantities. In the following sections we report the results obtained with the unselected sample.

3.3 Comparison with literature results

The results presented in this paper can be compared with those obtained by previous groups in the past. In particular, a natural comparison can be made with the work by Bianchini et al. (2018) who detected rotations in 11 GCs using only proper motions form the same data base adopted here. We restrict ourselves to those GCs with a 3σ detection in both works. Seven GCs have been found to rotate in both analyses (NGC 104, NGC 5139, NGC 5904, NGC

6273, NGC 6656, NGC 7078, and NGC 7089). Three GCs (NGC 5272, NGC 6752, and NGC 6809) also classified as rotating in both analyses have been excluded in our sample because of their low-rotation amplitude in proper motion which could be mimicked by small-scale systematics. In this regard, Bianchini et al. (2018) claimed that systematics should be negligible within the field of view covered by these clusters. However, as already reported in Section 3.2, although such a low-amplitude rotation cannot be excluded for these GCs, we conservatively exclude them from our final sample. We find only a 2σ (95.4 per cent $< P <$ 99.7 per cent) significant rotation signal in NGC 4372. This cluster is the one with the smallest rotation amplitude in the sample of Bianchini et al. (2018). Being at the border of the significance limits in both works, the actual rotation in this cluster is not clear. NGC 6553 and Ter 5 are not included in the sample analysed of Bianchini et al. (2018). For three clusters (NGC 2808, NGC 6205, and NGC 6626) we measured inclination angles larger than $i > 80^\circ$ implying a rotation signal almost entirely contained in the line-of-sight velocity space. Since the work by Bianchini et al. (2018) uses only proper motions, they are insensitive to the rotation in the plane perpendicular to the line of sight and it is therefore not surprising that they do not detect any significant rotation in these GCs, although they report a 2σ significance level for NGC 6205. For the remaining three GCs (NGC 6266, NGC 6397, and NGC 6541) Bianchini et al. (2018) found a 2σ rotation signal. Note that our work, being based on all the three velocity components, has a higher detection efficiency than that of Bianchini et al. (2018) and thus is able to detect rotation also in these clusters. The comparison between the estimated amplitudes, position, and inclination axis for the clusters in common is shown in Fig. 3. A good agreement is found for all these quantities.

The same conclusions hold for the rotation claimed by Gaia Collaboration (2018b) in the *Gaia* Science verification paper, who find rotation in eight GCs: five included in our final sample (NGC 104, NGC 5139, NGC 5904, NGC 6656, and NGC 7078) and three excluded in our analysis because of their low-rotation amplitudes (NGC 5272, NGC 6752, and NGC 6809; see above).

Recently, Vasiliev (2018) analysed *Gaia* proper motions in ∼80 Galactic GCs and studied their rotation pattern adopting stringent thresholds to account for the effect of systematic errors. We confirm the rotation detected by this author in the eight GCs for which he states a 3σ level detection. Of the 10 GCs with a 2σ level detection, five are classified as 'uncertain' in our work (NGC 5272, NGC 6093, NGC 6341, NGC 6752, and NGC 6809), three show a 2σ significant rotation (NGC 4372, NGC 5986, and NGC 6341), one is found to be non-rotating (NGC 6388) and one is not included in our sample (IC 1276). As for the Bianchini et al. (2018) work, no rotation could be detected by Vasiliev (2018) in the six rotating GCs with inclination angles $i > 65^\circ$ (NGC 2808, NGC 6205, NGC 6397, NGC 6541, NGC 6553, and NGC 6626), while Ter 5 is not included in his sample.

Among works based on line-of-sight velocities, Lane et al. (2010) analysed the kinematics of 10 GCs and found a significant rotation in three of them. We find the same rotation signal in two of them (NGC 104 and NGC 6656) while we do not obtain a significant detection in NGC 6121.

Bellazzini et al. (2012) merged literature data with their own results for a sample of 24 Galactic GCs. Although they do not report a list of significant rotators, 13 GCs of their sample have amplitudes at 3σ above the statistical errors. We find significant rotation for six of them (NGC 104, NGC 2808, NGC 5139, NGC 5904, NGC 6656, and NGC 7078), while we do not confirm rotation in the remaining seven (NGC 1851, NGC 3201, NGC 4590, NGC 6121, NGC 6388, NGC 6441, and NGC 6715), although NGC 3201 has a rotation signal at a 2σ significance level. They do not find rotation in NGC 6397. However, for this cluster we find a very small rotation amplitude in the radial component ($A \sin i \sim 0.46$ km s^{-1}; i.e. similar to their reported measurement error). It is therefore not surprising they were not able to detect such a small signal.

Fabricius et al. (2014) claimed the presence of rotation in all the 11 GCs of their sample. We confirm rotation for only three of them (NGC 5904, NGC 6205, and NGC 6626 i.e. those with the largest rotation amplitude in Fabricius et al. 2014), while four GCs (NGC 5272, NGC 6093, NGC 6218, and NGC 6341) were classified as 'uncertain' in our analysis. It is worth stressing that rotation in the work by Fabricius et al. (2014) is measured as a mean slope in the velocity field derived through integrated spectra of the cluster core. This technique can in principle be affected by spurious detections due to the inhomogeneous distribution of individual bright stars. While they report uncertainties as small as 0.1 km s^{-1} arcmin^{-1}, it is possible that their 100 per cent detection rate might be overestimated.

Lardo et al. (2015) analyse seven GCs and detect significant rotation in four of them. We confirm their result for NGC 2808 and NGC 7078 (those with the largest rotation amplitude in their sample), while we do not find any significant signal in NGC 1851 and NGC 5927.

Similarly, Kimmig et al. (2015) detected rotation in four GCs in common with our sample (NGC 104, NGC 5904, NGC 7078, and NGC 7089) and in NGC 5466 (for which we do not confirm rotation). On the other hand, the rotation signal they measured in NGC 2808 and NGC 6656 was not significant in their analysis, likely because of their small sample.

We confirm rotation in 9 among the 12 GCs in common with the study of Kamann et al. (2018) (NGC 104, NGC 2808, NGC 5139, NGC 5904, NGC 6266, NGC 6541, NGC 6656, NGC 7078, and NGC 7089) while we classified as 'uncertain' the detection in NGC 6093 and NGC 7099. We instead do not find any significant signal in NGC 1851. Note that the study by Kamann et al. (2018) uses several thousand stars per cluster being more sensitive than our study in those clusters with a small rotation amplitude and aligned with the line of sight. Moreover, the samples used by Fabricius et al. (2014) and Kamann et al. (2018) cover the innermost 30 arcsec of their GCs, while our work sample the clusters mainly outside their cores.

Finally, among the six GCs classified as rotating GCs by Ferraro et al. (2018) we find only a 2σ significant rotation in NGC 3201 and classified as 'uncertain' two of them (NGC 1904 and NGC 5272). No rotation has been instead found in NGC 288, NGC 362, and NGC 6171 in our analysis. Note that Ferraro et al. (2018) define a detection when a significant asymmetry in the velocity distribution about the rotation axis is apparent in any radial bin, while they report no significant signal when the entire sample is considered (like in our analysis).

The comparison with the above literature results is summarized in Table 3.

Other studies devoted to individual clusters detected rotation in many GCs of our final list: NGC 104 (Meylan & Mayor 1986; Strugatskaya 1988; Gebhardt et al. 1995; Gerssen et al. 2002; Anderson & King 2003), NGC 5139 (Woolley 1964; Merritt, Meylan & Mayor 1997; Norris et al. 1997; van Leeuwen et al. 2000; Reijns et al. 2006; van de Ven et al. 2006; Pancino et al. 2007; Sollima et al. 2009), NGC 5904 (Lanzoni et al. 2018), NGC 6397 (Gebhardt et al. 1995), NGC 6656 (Peterson & Cudworth 1994), NGC 7078 (Dubath & Meylan 1994; Gebhardt et al. 1994;

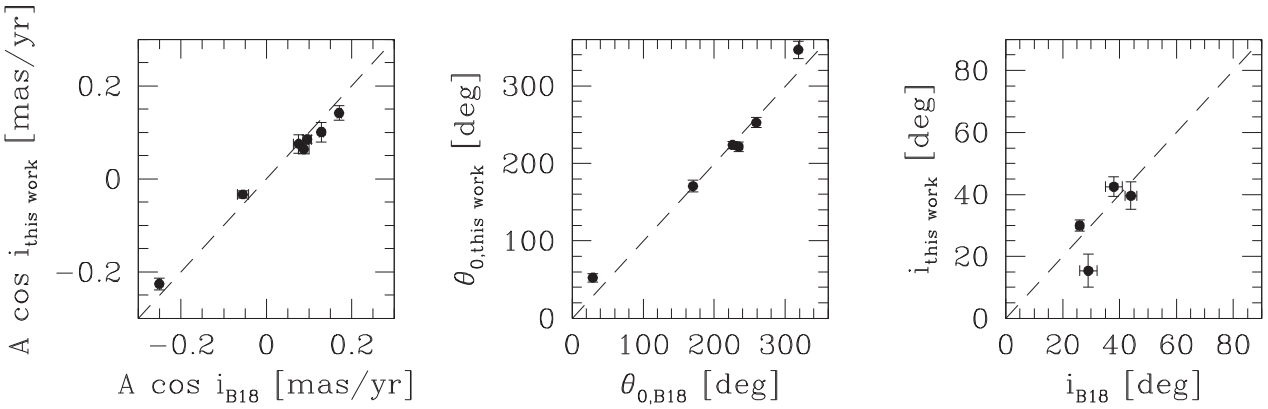

Figure 3. Comparison between the rotation amplitudes in the plane of the sky (left-hand panel), position angle (middle panel), and inclination angle (right-hand panel) of the rotation axis estimated by Bianchini et al. (2018) and this work. The dashed line marks the one-to-one relation in all panels.

Drukier et al. 1998), and NGC 7089 (Pryor et al. 1986). On the other hand, we detect a rotation at a 2σ level in NGC 3201 (Cote et al. 1995) and NGC 4372 (Kacharov et al. 2014), and an 'uncertain' classification has been given to NGC 5272 (Kadla & Strugatskaya 1985). We do not confirm instead the rotation found in NGC 5024 (Boberg et al. 2017), NGC 6388 (Lanzoni et al. 2013), and NGC 6121 (Malavolta et al. 2015).

4 DYNAMICAL MODELLING

The algorithm described in Section 3.1 provided a measure of the mean rotation amplitude in our sample of GCs. However, in a real cluster the rotation velocity depends on position. On the other hand, the efficiency of the radial sampling of our samples is given by the combination of the selection function of the considered data bases. These depend on many factors like the heliocentric distance, the crowding conditions, etc. resulting in an inhomogeneous sampling of the clusters. Thus, the derived mean amplitudes are biased estimates of the actual rotation of our GCs and should not be compared with each other. A more appropriate way to derive the characteristics of the rotation of our GCs is to compare our data set with suitable dynamical models. As specified in Section 2, for this comparison we used for each cluster the extended samples of stars i.e. those stars having at least one measure of their line-of-sight velocities or proper motions. Additionally, the surface-brightness profiles of Trager et al. (1995) have been employed as further constrains.

Many self-consistent models of rotating stellar systems have been developed in the past (e.g. Wilson 1975). These models are defined from a distribution function depending on two integrals of motions (energy and angular momentum along the rotation axis) which is integrated in a cylindrical coordinate system. Indeed, rotating stellar systems generally present a flattening along the direction of the rotation axis due to the kinetic energy excess along the radial direction in the equatorial plane produced by ordered motions. As a side effect, both the projected density profile and the resulting velocity distributions depend on the same model parameters. Unfortunately, the adopted set of structural and kinematic data has very different accuracies with the fractional uncertainty in the surface brightness being about one order of magnitude smaller than that in the velocity dispersion in the same radial intervals. As a consequence, the fit of the dynamical model is entirely dominated by the fine details of the surface-brightness profile while kinematics have only a little impact. In this case, it is possible to obtain a best fit to the data in which the distribution of velocities is poorly reproduced. However, differences in the projected density can be also produced by other factors (e.g. small variations in the shape of the adopted distribution function, tidal effects, etc.) which are out of control.

To overcome this problem, we constructed parametric models of rotating stellar systems by assuming a priori density profile and deriving kinematics from the Jeans equation, assuming spherical symmetry. Briefly, for an adopted density profile the associated profile of the second moment of the velocity $\langle v^2\rangle \equiv \langle v_\phi^2\rangle + \langle v_r^2\rangle + \langle v_\theta^2\rangle$ has been calculated using the Jeans equation in spherical coordinates (equation B1; here v_r, v_θ and v_ϕ are the velocity component in the radial, polar and azimuthal directions,[3] respectively). The relative contribution of ordered and random motions to $\langle v^2\rangle$ at a given position inside the cluster has been calculated adopting a parametric relation depending on the distance to the rotation axis.

$$f = \frac{\langle v_\phi\rangle^2}{\langle v_r^2\rangle + \langle v_\theta^2\rangle + \langle v_\phi^2\rangle} = \frac{b}{3}\,\frac{\exp(R/R_0)-1}{\exp(R/a\ R_0)+1}\,, \tag{4}$$

where b governs the strength of rotation, R_0 is a scale radius at which rotation approaches its maximum contribution to the kinetic energy, and a is a dampening factor at large radii. A comprehensive description of the modelling technique is provided in Appendix B.

Of course, the use of the Jeans equation does not ensure self-consistency (i.e. it is possible to obtain a model with a corresponding distribution function which is negative in some point of the energy-angular momentum space). Moreover, while spherical rotating models can exist (Lynden-Bell 1960), deviations from spherical symmetry have been observed in almost all GCs (White & Shawl 1987; Chen & Chen 2010). The models adopted here thus provide only an empirical representation of the rotation of GCs which is supported by a general physical justification.

The advantage of the above technique is that the density and velocity distribution profiles depend on non-degenerate sets of parameters. The fitting procedure has been performed in two subsequent steps: first, for each cluster we adopted the 3D density profile of the best-fitting King (1966) model (defined by the W_0 and r_c parameters from McLaughlin & van der Marel 2005) and we then searched the combination of parameters (a, b, R_0) which maximize the likelihood of equation 3, where the values of $\overline{v_{j,i}}$ and $\sigma_{j,i}$ were calculated from equation B7. A Markov Chain Monte

[3] In this notation v_ϕ corresponds to the rotational velocity.

Table 3. Detection of rotation in GCs from literature results: checkmarks, crosses, and tildes mark positive, negative, and 2σ detections, respectively. Checkmarks within parenthesis mark those GCs with uncertain detections found in this work. References: Lane et al. (2010, L10), Bellazzini et al. (2012, B12), Fabricius et al. (2014, F14), Lardo et al. (2015, L15), Kimmig et al. (2015, K15), Kamann et al. (2018, K18), Ferraro et al. (2018, F18), Gaia Collaboration (2018b, G18), Bianchini et al. (2018, B18), Vasiliev (2018, K18). Only GCs with at least a 2σ detection have been listed.

Name	L10	B12	F14	L15	K15	K18	F18	G18	B18	V18	This work
NGC 104	✓	✓			✓	✓		✓	✓	✓	✓
NGC 288	X	X			X		✓		X	X	X
NGC 362					X	~	✓		X	X	X
NGC 1261							~				X
NGC 1851		✓		✓		✓			~	X	X
NGC 1904		X					✓		X		(✓)
NGC 2808		✓		✓	X	✓			X	X	✓
NGC 3201		✓				✓	✓		~	X	~
NGC 4372				X					✓	~	~
NGC 4590	X	✓			X				X	X	X
NGC 5024	X	X	✓		X						~
NGC 5139		✓				✓		✓	✓	✓	✓
NGC 5272			✓		X		✓	✓	✓	~	(✓)
NGC 5286									~	X	X
NGC 5466					✓						X
NGC 5824											(✓)
NGC 5904		✓	✓		✓	✓		✓	✓	✓	✓
NGC 5927				✓			~		X	X	X
NGC 5986									X	X	~
NGC 6093			✓			✓			~	X	(✓)
NGC 6121	✓	✓			~	~			~	X	X
NGC 6171		~					✓		X	X	X
NGC 6205			✓						~	X	✓
NGC 6218	X	X	✓		X				X	X	(✓)
NGC 6254		X	✓			✓	~		~	X	X
NGC 6266						✓			~	✓	✓
NGC 6273									✓	✓	✓
NGC 6293						✓				X	
NGC 6341			✓		~				X	X	(✓)
NGC 6388		✓				✓			X	X	X
NGC 6397		X							~	X	✓
NGC 6402					X				~	X	~
NGC 6441		✓			X	~				X	X
NGC 6496							~				X
NGC 6522						~			X		X
NGC 6539									~	X	~
NGC 6541						✓			~	X	✓
NGC 6553										X	✓
NGC 6626			✓						X	X	✓
NGC 6656	✓	✓			X	✓		✓	✓	✓	✓
NGC 6681						~			X	X	
NGC 6715		✓			X					X	X
NGC 6723							~			X	X
NGC 6752	X	X		X	X	~		✓	✓	~	(✓)
NGC 6779			✓						~	X	X
NGC 6809	~	~			~			✓	✓	~	(✓)
NGC 6838		~			X				X	X	~
NGC 6934			✓		X						
NGC 7078		✓		✓	✓	✓		✓	✓	✓	✓
NGC 7089					✓	✓			✓	✓	✓
NGC 7099	X	X			X	~			X	X	(✓)
Terzan 5											✓

Carlo has been used to survey the parameter space searching for the parameters a, b, and R_0 providing the maximum likelihood. The position (θ_0) and inclination (i) angles or the rotation axis have been fixed to those calculated through the algorithm described in Section 3.1. Indeed, tests performed on the synthetic catalogues (see Section 3.1) indicate that the adopted algorithm provides unbiased estimates of these quantities while systematic offsets are obtained by leaving them as free parameters.

The best-fitting models for the 15 GCs of our final sample are shown in Figs 4 and 5. In these figures, the line-of-sight velocity dispersion and rotation profiles have been computed (for visualization purposes only) by binning the samples of line-of-sight

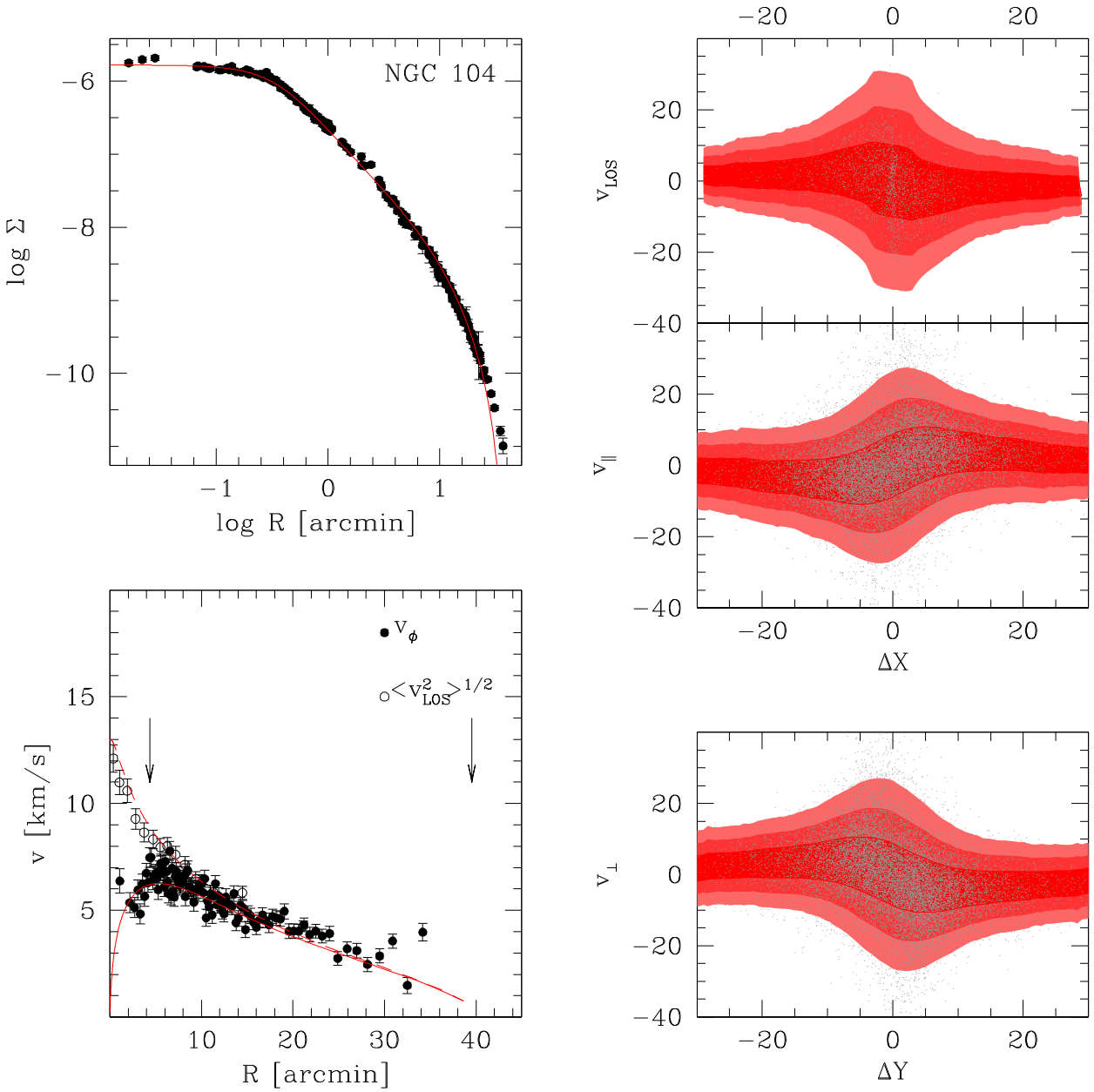

Figure 4. Best-fitting model of NGC 104 (the entire set of models for the 15 GCs with positive detection of rotation is available in the online version of the paper). Top left-hand panel: projected density profile, black points represent the profile of Trager, King & Djorgovski (1995). Bottom left-hand panel: rotation (solid line) and velocity dispersion (dashed line) profiles. Filled and open dots represent the corresponding observed profiles. The location of the half-mass and tidal radii are marked by arrows. Right-hand panels: distributions of velocities in the three components as a function of the distance along (ΔY) and from (ΔX) the rotation axis. Red shaded area indicates the 1, 2, and 3σ intervals. Grey points mark observational data. For clarity, only velocities with errors smaller than 5 km s^{-1} are plotted.

velocities and proper motions and applying the technique described in Section 3.1 to individual bins. The distribution of velocities in the three components are plotted as a function of the distance along (ΔY) and from (ΔX) the rotation axis

$$\Delta X = -R \sin(\theta - \theta_0)$$
$$\Delta Y = R \cos(\theta - \theta_0)$$

From Figs 4 and 5 it is apparent that while the considered models provide a good fit to the density and rotational/dispersion velocity profiles in most GCs of our sample, significant discrepancies are noticeable for a few clusters (e.g. NGC 6656 and Ter 5). Note however that in these GCs the mismatch between models and data is confined to the outer bins containing only a few stars. Instead, the model parameters are fitted using individual velocities so that the strongest constraint is provided by regions where more data points are available.

Usually, the ratio between the projected rotation amplitude and the central line-of-sight velocity dispersion ($v_{\phi,\max}/\sigma_0$) is used as an indicator of the relative importance of rotation (Davies et al. 1983). However, the use of this ratio has many drawbacks since it does not account for the different cluster concentrations and different shapes of the rotation curve (Binney 2005). To overcome this limitation and to assess the strength of rotation for each cluster, we calculated

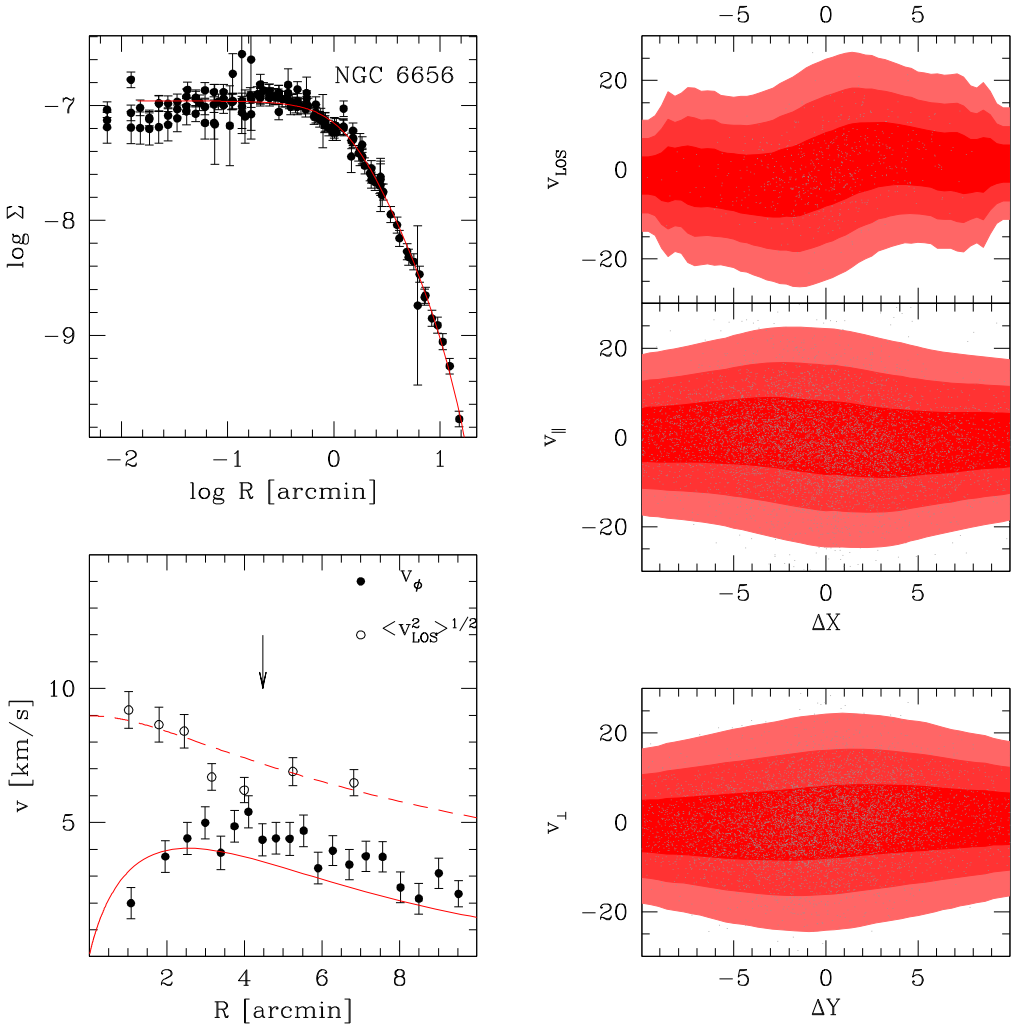

Figure 5. Same as Fig. 4 for NGC 6656.

the fraction of kinetic energy in rotational motions $\xi \equiv \langle v_\phi^2 \rangle / \langle \sigma^2 \rangle$ of the corresponding best-fitting model. These fractions are listed in Table 2 . Note that ξ is a global parameter and it is therefore a more robust rotation indicator in comparison with other estimators like e.g. $v_{\phi,\max}/\sigma_0$, which are measured at different distances from the centre, depend on the binning and use small subsamples of stars.

Moreover, we also calculated the model rotation period at the half-mass radius as

$$P_{\rm rot} = \frac{2\pi r_{\rm h}}{v_\phi(r_{\rm h})}. \quad (5)$$

5 GLOBULAR CLUSTER PARAMETER CORRELATIONS

The values of ξ calculated in the previous section have been used to search for correlations with other general and dynamical parameters. We considered the horizontal branch morphology parameter (*HBR*; from Lee, Demarque & Zinn 1994), Galactocentric distance, height above the Galactic plane ($R_{\rm GC}$, Z; from Harris 1996) mass, half-mass radius, half-mass relaxation time (M, $r_{\rm h}$, $t_{\rm rh}$; from Baumgardt & Hilker 2018) metallicity (Fe/H; from Carretta et al. 2009), ellipticity (ϵ; from Chen & Chen 2010), and destruction rate (ν defined as the inverse of the time needed by the cluster to completely dissolve; from Baumgardt et al. 2019). Ellipticities have been deprojected using the technique described in Cappellari et al. (2007) and assuming the same inclination angles of the rotation axis, based on the hypothesis that rotation and flattening are linked.

To evaluate the significance of such correlations we performed both the Spearman rank correlation test and a permutation test for Pearson's weighted correlation coefficient. For the latter test, we assume ξ as the dependent variable and constructed 10^4 random permutation of each independent variable. For each set the weighted Pearson's correlation coefficient has been calculated. The fraction of randomized sets with a correlation coefficient smaller than the one measured on the original data gives the probability that the two variables are correlated.

The entire set of correlations is shown in Fig. 6 together with the corresponding correlation probabilities. Unfortunately, given the small size of our data base, we are not able to confirm or exclude any of the considered correlations at a significant confidence level. On average, both the performed tests provide similar results with the Spearman test giving generally larger significance levels than the permutation one. The largest correlation probabilities (still below the 3σ level) are those with the half-mass radius and relaxation time, in agreement with what was found by Kamann et al. (2018) and Bianchini et al. (2018). Also noticeable is the anticorrelation

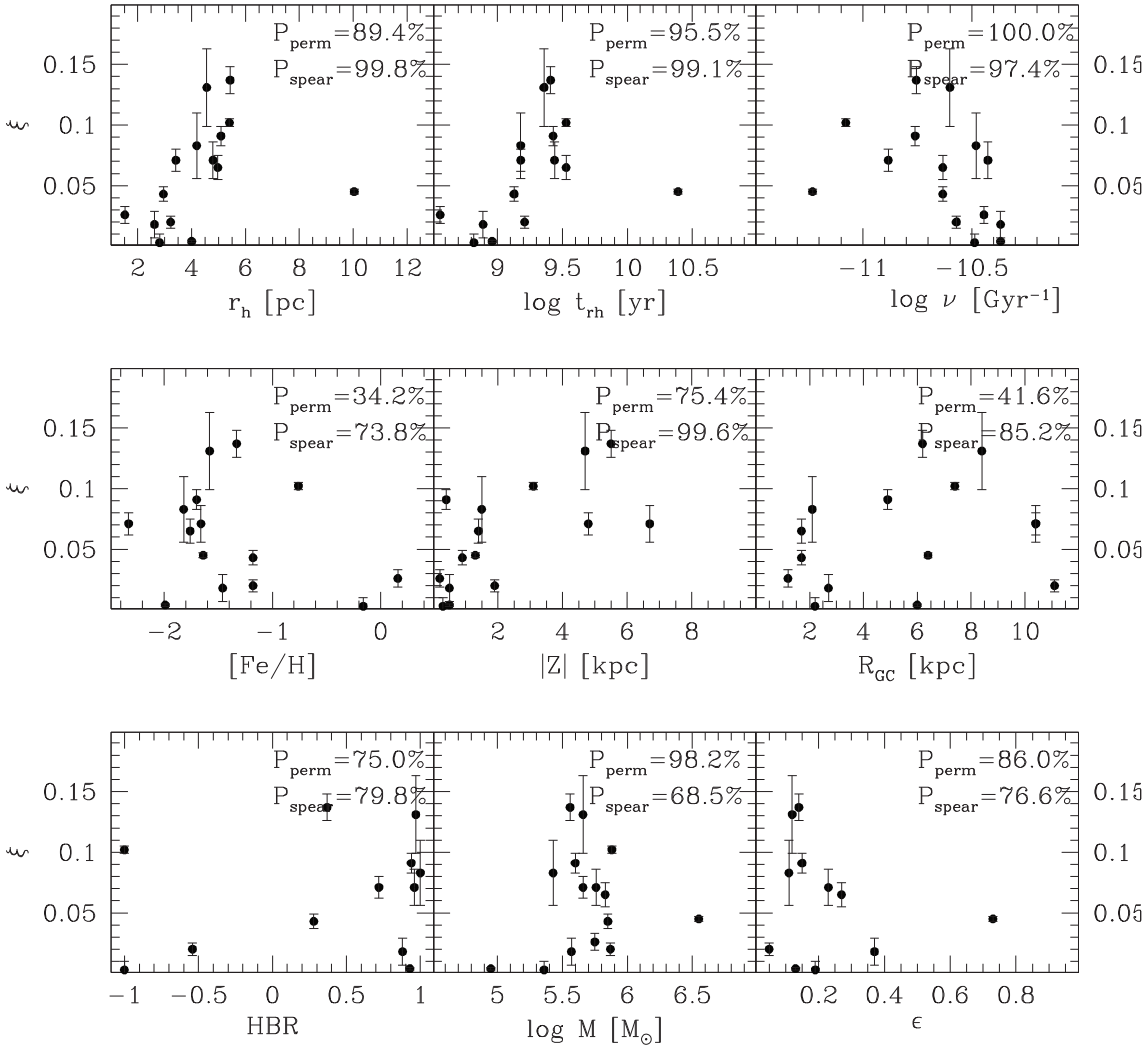

Figure 6. Correlation between the fraction of rotational kinetic energy (ξ) and various parameters. The correlation probability is indicated in each panel.

with the destruction rate. An interesting outlier in the above planes is NGC 5139 showing a relatively small rotation strength in spite of its long half-mass relaxation time and low destruction rate.

A relatively small correlation probability is instead that with the ellipticity. To further investigate the relation between rotation and flattening, we also calculated the angle in the plane of the sky between the position angle of the rotation axis with the direction of the isophotal minor axis (from Chen & Chen 2010). A one-tailed Kolmogorov–Smirnov indicates a probability of 6.2 per cent that such a correlation occurs by chance. It is worth noting that the ellipticity of Chen & Chen (2010), based on star counts in infrared images, are less affected by foreground extinction than the optical data, but more affected by individual star count numbers and by features at larger radius such as tidal tails or outer stretching of the cluster distribution. So, we also used the ellipticities provided by White & Shawl (1987) which are based on the overall integrated light profiles and are therefore more representative of the (inner) brightest parts of the clusters. With this data set we find a more significant correlation probability (99.8 per cent and 85.7 per cent according to the permutation and the Spearman tests, respectively) although the alignment of the minor and rotation axes is not significant (11.6 per cent that the angle difference is extracted from a random distribution).

An interesting test for the impact of the tidal field on internal rotation has been done by calculating the angle between the rotation axes and the orbital poles of the GCs in our sample. For this purpose, we computed the orientation of the axes in the Galactic reference system and calculated the angles with the North (South) Galactic pole if the cluster has a positive (negative) angular momentum along the direction perpendicular to the Galactic plane (from Gaia Collaboration 2018b). Indeed, all the 15 GCs of our sample move in a region of the Galactic potential which is dominated by the disc, and their orbital poles oscillate during the cluster orbit around the Galactic pole. Therefore, the average orientation of the orbital pole over many orbits is always pointed towards the Galactic pole. A one-tailed Kolmogorov–Smirnov indicates a probability of 1.5 per cent that such an angle is distributed following a constant probability per solid angle corresponding to a random orientation ($P(\Delta i) \propto \sin \Delta i$). We also calculated the angle between the rotation axes and the instantaneous orbital poles, defined as the normal vectors to the planes containing the present-day position and velocity vectors. Also in this case, we found a probability of 11.3 per cent that such an angle comes from a random orientation of the rotation axes.

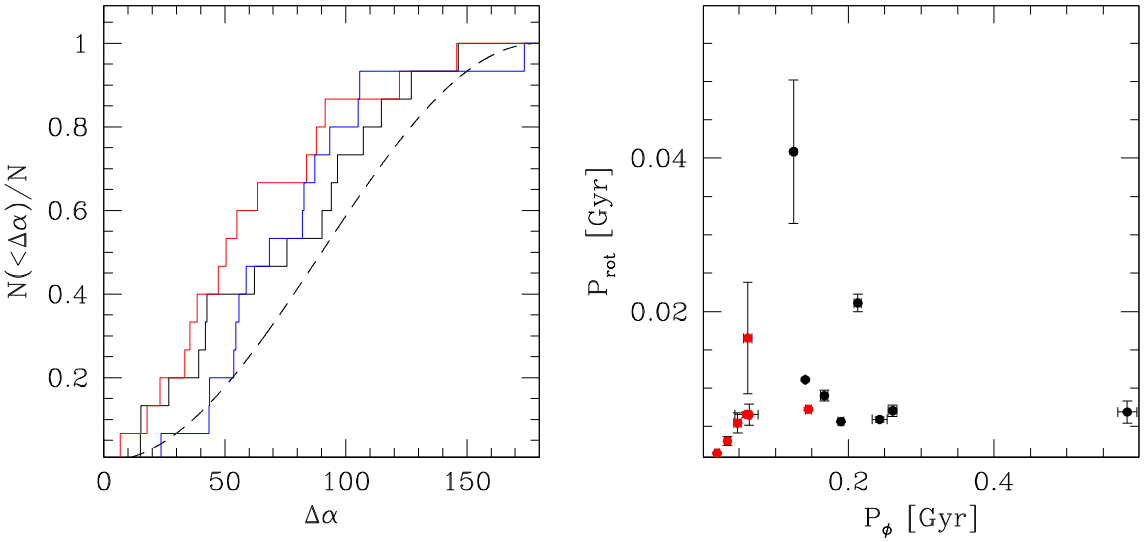

Figure 7. Left-hand panel: cumulative distribution of the angle between the rotation axis and the plane of the sky (black solid line), the Galactic pole (red line), and the present-day orbital pole (blue line). The behaviour of a randomly oriented distribution is shown by the dashed line. Right-hand panel: comparison between the rotation period at the half-mass radius and the orbital period. Red and black dots mark GCs with Galactocentric distances smaller and larger than 6 kpc, respectively.

For comparison, if we perform the same test on the inclination angle with respect to the plane of the sky, and neglecting the dependence of the detection efficiency on it, the probability that it is randomly distributed is 19.4 per cent (see the left-hand panel of Fig. 7).

Finally, in the right-hand panel of Fig. 7 we compare the rotation period at the half-mass radius with the cluster orbital period (from Gaia Collaboration 2018b). While these two variables are not significantly correlated when considering the entire sample (the permutation and Spearman tests give probabilities of 70.5 per cent and 92.0 per cent, respectively), a strong correlation of these two variables is apparent for GCs with $R_{\rm GC} < 6$ kpc. A least-square fit to this subsample of clusters gives a ratio $P_\phi/P_{\rm rot} = 9.2 \pm 2.5$. Note however that, as it is immediately apparent from equation 5, the rotation period at the half-mass radius is proportional to the half-mass radius itself. On the other hand, it is well known that a half-mass radius versus Galactocentric distance relation is present among Galactic GCs (van den Bergh, Morbey & Pazder 1991), with the GCs at large distances from the Galactic centre (i.e. those which take a long time to complete their orbits) being on average more extended. So, since both the orbital and the rotational periods depend on the Galactocentric distance, the correlation between these two time-scales could be spurious. Indeed, this correlation is not associated with an alignment of the rotation axes with the orbital poles: if we restrict the sample to GCs with $R_{\rm GC} < 6$ kpc, the probability that the angle between these two directions is randomly distributed increases to 2.4 per cent.

6 SUMMARY

We constructed the most extensive set of kinematic information for stars in 62 Galactic GCs, sampling ∼40 per cent of the GC system of the Milky Way, matching *Gaia* proper motions with the most comprehensive survey of line-of-sight velocities. We explored for each analysed cluster the velocity distribution in the three components searching for statistically significant signals of rotation. We found robust evidence of rotation in 15 GCs of our sample at an amplitude which cannot be explained by neither random nor systematic errors. For nine more GCs we found a signal of rotation mainly in the plane of the sky at a level below the claimed amplitude of systematic uncertainties possibly present in the *Gaia* catalogue. Although the presence of a genuine rotation is well possible in these GCs, we cannot exclude that this evidence might be spuriously produced by the patchy distribution pattern of systematics. The present analysis adds an important piece of information to the recent work by Bianchini et al. (2018) since taking advantage of the information on the velocity along the line of sight, (i) it has a higher efficiency in detecting GCs rotating with large inclination angles, and (ii) it allows to determine the inclination of the rotation axis with respect to the line of sight.

The relative strength of ordered over random motions (ξ) has been also calculated by means of the comparison with dynamical models. The derived values of ξ appear to weakly correlate with the half-mass relaxation time, with the GCs with longer relaxation times rotating faster. This evidence, already noticed by Kamann et al. (2018) and Bianchini et al. (2018), is in agreement with the predictions of *N*-body simulations (Tiongco et al. 2017). It could suggest a primordial origin for the rotation of these stellar systems which is progressively erased by both internal and external dynamical processes. Indeed, two-body relaxation tend to randomize the orbits of stars thus erasing the effect of ordered motions. In this picture, less evolved GCs (i.e. those with a longer half-mass relaxation time) still maintain the evidence of their original rotation. Moreover, the observed anticorrelation between ξ and the destruction rate suggests that GCs subject to a fast destruction process lost much of their original angular momentum. The massive GC NGC 5139 presents a remarkably small rotation strength in spite of its long half-mass relaxation time and low destruction rate. This finding suggests peculiar initial conditions for this stellar system characterized by a relatively small primordial rotation.

We also checked the importance of the Galactic tidal field in determining the rotation of GCs. The comparison between the orientation of the rotation axis with the average and the instantaneous orbital pole does not provide any significant conclusion. It is interesting to notice the strong correlation between the rotation period at the half-mass with the orbital period of those GCs at small Galactocentric distances ($R_{GC} < 6$ kpc). However, although a synchronization of internal and orbital rotation is predicted by simulations (Tiongco et al. 2016, who found however a much smaller ratio $P_\phi/P_{rot} \sim 0.5$ close to the tidal radius), this evidence could be spuriously produced by the half-mass radius versus Galactocentric distance relation present in the Galactic GC system (van den Bergh et al. 1991). This is also suggested by the lack of any significant alignment of the rotation axis with the orbital poles in this subsample of clusters. Note that tidal effects are expected to be effective in creating a retrograde rotation only at large distances from the cluster centre (Vesperini et al. 2014), while our data sample mainly the inner region of GCs. Therefore, the lack of a clear correlation between the rotation properties of our GCs and the strength of the tidal field is not surprising. In this context, the rotation found in the GCs of our sample is more likely reminiscent of their initial conditions.

At odds with what was found by Fabricius et al. (2014) and Kamann et al. (2018), we do not find evidence of a link between rotation and flattening, in terms of neither the correlation between the rotation strength and the deprojected ellipticity nor the alignment of the rotation axis with the isophotal minor axis. The lack of such a correlation, already reported by Bellazzini et al. (2012) and Lardo et al. (2015), could be due to the effect of anisotropy and tidal distortions in shaping the outermost regions of the clusters which introduce a spread in the ξ diagram (see Kamann et al. 2018).

Unfortunately, all the conclusions drawn on the basis of the explored correlations suffer from the small size of our sample. In this situation, it is well possible that some of the explored correlations are actually real but remain hidden in the Poisson noise resulting statistically non-significant. An important improvement is expected in the near future when the next *Gaia* releases will be available. According to the performance prediction of the *Gaia* consortium, the end of mission accuracy should improve by a factor of two and the amplitude of systematics is expected to significantly decrease. In that condition, the same analysis performed here should be able to clarify the presence of rotation in the GCs with uncertain detections and to construct a much larger sample of rotating GCs which can allow to verify the correlations analysed in this work.

ACKNOWLEDGEMENTS

We warmly thank Michele Bellazzini and Paolo Bianchini for useful discussions. We also thank the anonymous referee for his/her helpful comments and suggestions.

REFERENCES

Anderson J., King I. R., 2003, AJ, 126, 772
Arenou F. et al., 2018, A&A, 616, A17
Baumgardt H., 2017, MNRAS, 464, 2174
Baumgardt H., Hilker M., 2018, MNRAS, 478, 1520
Baumgardt H., Hilker M., Sollima A., Bellini A., 2019, MNRAS, 482, 5138
Bellazzini M., Bragaglia A., Carretta E., Gratton R. G., Lucatello S., Catanzaro G., Leone F., 2012, A&A, 538, A18
Bellini A., Bianchini P., Varri A. L., Anderson J., Piotto G., van der Marel R. P., Vesperini E., Watkins L. L., 2017, ApJ, 844, 167
Bianchini P., van der Marel R. P., del Pino A., Watkins L. L., Bellini A., Fardal M. A., Libralato M., Sills A., 2018, MNRAS, 481, 2125
Binney J., 2005, MNRAS, 363, 937
Boberg O. M., Vesperini E., Friel E. D., Tiongco M. A., Varri A. L., 2017, ApJ, 841, 114
Cappellari M. et al., 2007, MNRAS, 379, 418
Carretta E., Bragaglia A., Gratton R., D'Orazi V., Lucatello S., 2009, A&A, 508, 695
Chen C. W., Chen W. P., 2010, ApJ, 721, 1790
Cote P., Welch D. L., Fischer P., Gebhardt K., 1995, ApJ, 454, 788
Davies R. L., Efstathiou G., Fall S. M., Illingworth G., Schechter P. L., 1983, ApJ, 266, 41
Drukier G. A., Slavin S. D., Cohn H. N., Lugger P. M., Berrington R. C., Murphy B. W., Seitzer P. O., 1998, AJ, 115, 708
Dubath P., Meylan G., 1994, A&A, 290, 104
Fabricius M. H. et al., 2014, ApJ, 787, L26
Ferraro F. R. et al., 2018, ApJ, 860, 50
Gaia Collaboration, 2018a, A&A, 616, A1
Gaia Collaboration, 2018b, A&A, 616, A12
Gebhardt K., Pryor C., Williams T. B., Hesser J. E., 1994, AJ, 107, 2067
Gebhardt K., Pryor C., Williams T. B., Hesser J. E., 1995, AJ, 110, 1699
Gerssen J., van der Marel R. P., Gebhardt K., Guhathakurta P., Peterson R. C., Pryor C., 2002, AJ, 124, 3270
Goldsbury R., Heyl J., Richer H., 2013, ApJ, 778, 57
Harris W. E., 1996, AJ, 112, 1487
Hénault-Brunet V., Gieles M., Sollima A., Watkins L. L., Zocchi A., Claydon I., Pancino E., Baumgardt H., 2019, MNRAS, 483, 1400
Henon M., 1970, A&A, 9, 24
Kacharov N. et al., 2014, A&A, 567, A69
Kadla Z. I., Strugatskaya A. A., 1985, Pis'ma Astron. Zh., 11, 670
Kamann S. et al., 2018, MNRAS, 473, 5591
Keenan D. W., Innanen K. A., 1975, AJ, 80, 290
Kimmig B., Seth A., Ivans I. I., Strader J., Caldwell N., Anderton T., Gregersen D., 2015, AJ, 149, 53
King I. R., 1966, AJ, 71, 64
Lane R. R. et al., 2010, MNRAS, 406, 2732
Lanzoni B. et al., 2013, ApJ, 769, 107
Lanzoni B. et al., 2018, ApJ, 861, 16
Lardo C. et al., 2015, A&A, 573, A115
Lee Y.-W., Demarque P., Zinn R., 1994, ApJ, 423, 248
Libralato M. et al., 2018, ApJ, 854, 45
Lindegren L. et al., 2018, A&A, 616, A2
Lynden-Bell D., 1960, MNRAS, 120, 204
Malavolta L., Piotto G., Bedin L. R., Sneden C., Nascimbeni V., Sommariva V., 2015, MNRAS, 454, 2621
Mapelli M., 2017, MNRAS, 467, 3255
Massari D., Bellini A., Ferraro F. R., van der Marel R. P., Anderson J., Dalessandro E., Lanzoni B., 2013, ApJ, 779, 81
McLaughlin D. E., van der Marel R. P., 2005, ApJS, 161, 304
Merritt D., Meylan G., Mayor M., 1997, AJ, 114, 1074
Meylan G., Mayor M., 1986, A&A, 166, 122
Norris J. E., Freeman K. C., Mayor M., Seitzer P., 1997, ApJ, 487, L187
Pancino E., Galfo A., Ferraro F. R., Bellazzini M., 2007, ApJ, 661, L155
Peterson R. C., Cudworth K. M., 1994, ApJ, 420, 612
Pryor C., McClure R. D., Fletcher J. M., Hartwick F. D. A., Kormendy J., 1986, AJ, 91, 546
Reijns R. A., Seitzer P., Arnold R., Freeman K. C., Ingerson T., van den Bosch R. C. E., van de Ven G., de Zeeuw P. T., 2006, A&A, 445, 503
Robin A. C., Reylé C., Derrière S., Picaud S., 2003, A&A, 409, 523
Sollima A., Bellazzini M., Smart R. L., Correnti M., Pancino E., Ferraro F. R., Romano D., 2009, MNRAS, 396, 2183
Sollima A., Baumgardt H., Zocchi A., Balbinot E., Gieles M., Hénault-Brunet V., Varri A. L., 2015, MNRAS, 451, 2185
Strugatskaya A. A., 1988, PAZh, 14, 31
Tiongco M. A., Vesperini E., Varri A. L., 2016, MNRAS, 461, 402

Tiongco M. A., Vesperini E., Varri A. L., 2017, MNRAS, 469, 683
Tiongco M. A., Vesperini E., Varri A. L., 2018, MNRAS, 475, L86
Trager S. C., King I. R., Djorgovski S., 1995, AJ, 109, 218
van de Ven G., van den Bosch R. C. E., Verolme E. K., de Zeeuw P. T., 2006, A&A, 445, 513
van den Bergh S., Morbey C., Pazder J., 1991, ApJ, 375, 594
van Leeuwen F., Le Poole R. S., Reijns R. A., Freeman K. C., de Zeeuw P. T., 2000, A&A, 360, 472
Vasiliev E., 2018, preprint (arXiv:1811.05345)
Vasiliev E., 2019, MNRAS, 484, 2832
Vesperini E., Varri A. L., McMillan S. L. W., Zepf S. E., 2014, MNRAS, 443, L79
White R. E., Shawl S. J., 1987, ApJ, 317, 246
Wilson C. P., 1975, AJ, 80, 175
Woolley R. V. D. R., 1964, Nature, 203, 961

SUPPORTING INFORMATION

Supplementary data are available at *MNRAS* online.

Figure 2. Distribution of the three velocity components as a function of the position angle for NGC 104 (the entire set of best fits for the 15 GCs with positive detection of rotation is available in the online version of the paper).
Figure 4. Best-fitting model of NGC 104 (the entire set of models for the 15 GCs with positive detection of rotation is available in the online version of the paper).

Please note: Oxford University Press is not responsible for the content or functionality of any supporting materials supplied by the authors. Any queries (other than missing material) should be directed to the corresponding author for the article.

APPENDIX A: DERIVATION OF THE ROTATION VELOCITY COMPONENTS

Consider a reference frame defined such that a cluster rotates clockwise in the x–y plane with the z-axis directed in towards the direction of the angular momentum. The systemic velocities along the three components can be written as

$$v_x = \omega y$$
$$v_y = -\omega x$$
$$v_z = 0$$

where $\omega \equiv \omega(x, y, z)$ is the angular velocity. The velocity components measured by an observer looking at the cluster from an inclined perspective (v_X, v_Y, v_Z) can be obtained by sequentially applying two rotations along the x- and z-axes by angles i and θ_0, respectively

$$v_X = v_x \cos\theta_0 - v_y \sin\theta_0 \cos i + v_z \sin\theta_0 \sin i = \omega\,(x \sin\theta_0 \cos i + y \cos\theta_0)$$

$$v_Y = v_x \sin\theta_0 + v_y \cos\theta_0 \cos i - v_z \cos\theta_0 \sin i = -\omega\,(x \cos\theta_0 \cos i - y \sin\theta_0)$$

$$v_Z = v_y \sin i + v_z \cos i = -\omega\, x \sin i\,. \tag{A1}$$

Defining the position angle θ anticlockwise from the Y-axis we have

$$X = -R \sin\theta \qquad Y = R \cos\theta$$

where $R = \sqrt{X^2 + Y^2}$ is the projected distance from the cluster centre. The coordinate transformation between the two reference systems are

$$x = X \cos\theta_0 + Y \sin\theta_0 = -R \sin(\theta - \theta_0)$$

$$y = -X \sin\theta_0 \cos i + Y \cos\theta_0 \cos i + Z \sin i = R \cos(\theta - \theta_0) \cos i + Z \sin i$$

$$z = X \sin\theta_0 \sin i - Y \cos\theta_0 \sin i + Z \cos i = -R \cos(\theta - \theta_0) \sin i + Z \cos i\,. \tag{A2}$$

Consider the projections of the velocity vector in the plane of the sky in the directions parallel and perpendicular to the rotation axis

$$v_\parallel = -v_X \sin\theta_0 + v_Y \cos\theta_0$$

$$v_\perp = v_X \cos\theta_0 + v_Y \sin\theta_0\,. \tag{A3}$$

Combining equations A1, A2, and A3 we finally find

$$v_Z = \omega\, R \sin(\theta - \theta_0) \sin i$$

$$v_\parallel = \omega\, R \sin(\theta - \theta_0) \cos i$$

$$v_\perp = \omega\,[R \cos(\theta - \theta_0) \cos i + Z \sin i]\,.$$

APPENDIX B: PARAMETRIC JEANS MODELS OF ROTATING SPHERICAL SYSTEMS

Consider the Jeans equation in spherical polar coordinates (r, θ, ϕ)

$$\frac{\delta\rho\langle v_{\rm r}^2\rangle}{\delta r} + \frac{1}{r}\frac{\delta\langle v_{\rm r} v_\theta\rangle}{\delta\theta} + \frac{\rho}{r}(2\langle v_{\rm r}^2\rangle - \langle v_\theta^2\rangle - \langle v_\phi^2\rangle + \langle v_{\rm r} v_\theta\rangle \cot\theta) = -\rho\frac{\delta\Phi}{\delta r}$$

$$\frac{\delta\langle v_{\rm r} v_\theta\rangle}{\delta r} + \frac{1}{r}\frac{\delta\rho\langle v_\theta^2\rangle}{\delta\theta} + \frac{\rho}{r}[3\langle v_{\rm r} v_\theta\rangle + (\langle v_\theta^2\rangle - \langle v_\phi^2\rangle)\cot\theta] = -\frac{\rho}{r}\frac{\delta\Phi}{\delta\theta}\,, \tag{B1}$$

where ρ is the 3D density, $v_{\rm r}$, v_θ, and v_ϕ are the velocities along the three components, r is the distance from the cluster centre, and Φ is the gravitational potential.

An obvious solution can be found by assuming

$$\langle v_{\rm r} v_\theta\rangle = 0$$

$$\langle v_{\rm r}^2\rangle = \langle v_\theta^2\rangle = \langle v_\phi^2\rangle$$

$$\frac{\delta\rho}{\delta\theta} = \frac{\delta\Phi}{\delta\theta} = \frac{\delta\langle v_{\rm r}^2\rangle}{\delta\theta} = 0\,. \tag{B2}$$

Thus, equation B1 reduces to the spherical Jeans equation

$$\frac{\delta\rho\langle v_{\rm r}^2\rangle}{\delta r} = -\rho\frac{\delta\Phi}{\delta r} \tag{B3}$$

The second velocity moments can be written separating the contribution of random and systematic motions assuming

$$\langle v_{\rm r}^2\rangle = \sigma_r^2$$
$$\langle v_\phi^2\rangle = \sigma_\phi^2 + \langle v_\phi\rangle^2 . \tag{B4}$$

We adopted an empirical relation linking the fraction of kinetic energy in rotational motion as a function of the distance to the rotation axis.

$$f = \frac{\langle v_\phi\rangle^2}{\langle v_{\rm r}^2\rangle + \langle v_\theta^2\rangle + \langle v_\phi^2\rangle} = \frac{b}{3}\,\frac{\exp(R/R_0)-1}{\exp(R/a\ R_0)+1}\,, \tag{B5}$$

where b governs the strength of rotation, R_0 is a scale radius at which rotation approaches its maximum contribution to the kinetic energy, and a is a dampening factor at large radii.

From equations B2, B4, and B5 we have

$$\sigma_\phi^2 = (1-3f)\,\sigma_r^2$$
$$\langle v_\phi\rangle^2 = 3f\ \sigma_r^2 . \tag{B6}$$

For a given density profile, the potential derivative is given by the gravitational acceleration

$$\frac{\delta\Phi}{\delta r} = -\frac{4\pi G}{r^2}\int_0^r \rho(r')r'^2\,{\rm d}r'$$

while the velocity dispersions in the r and ϕ components, as well as the mean rotational velocity can be calculated from equations B3 and B6.

For a given density profile and a combination of parameters (a, b, R_0) the ratio between rotational and overall kinetic energy is given by

$$\xi \equiv \frac{\langle\langle v_\phi\rangle^2\rangle}{\langle 3\ \sigma_r^2\rangle} = \frac{\int_0^{r_t}\int_0^{\sqrt{r_t^2-z^2}} R\rho f\sigma_r^2\,{\rm d}R\,{\rm d}z}{\int_0^{r_t}\int_0^{\sqrt{r_t^2-z^2}} R\rho\sigma_r^2\,{\rm d}R\,{\rm d}z}\,.$$

The mean velocities and dispersions along the projected components ($\perp$, $\shortparallel$, LOS) can be calculated as a function of the inclination angle i

$$\langle v_\perp\rangle = \frac{1}{\Sigma}\int_{-\infty}^{+\infty}\rho\ \langle v_\phi\rangle\frac{y\cos i + z\sin i}{\sqrt{(y\cos i + z\sin i)^2 + x^2}}\,{\rm d}z$$
$$\langle v_\shortparallel\rangle = -\frac{1}{\Sigma}\int_{-\infty}^{+\infty}\rho\ \langle v_\phi\rangle\frac{x\cos i}{\sqrt{(y\cos i + z\sin i)^2 + x^2}}\,{\rm d}z$$
$$\langle v_{\rm LOS}\rangle = -\frac{1}{\Sigma}\int_{-\infty}^{+\infty}\rho\ \langle v_\phi\rangle\frac{x\sin i}{\sqrt{(y\cos i + z\sin i)^2 + x^2}}\,{\rm d}z$$
$$\sigma_\perp^2 = \frac{1}{\Sigma}\int_{-\infty}^{+\infty}\rho\ \sigma_r^2\,{\rm d}z - \langle v_\perp\rangle^2$$
$$\sigma_\shortparallel^2 = \frac{1}{\Sigma}\int_{-\infty}^{+\infty}\rho\ \sigma_r^2\,{\rm d}z - \langle v_\shortparallel\rangle^2$$
$$\sigma_{\rm LOS}^2 = \frac{1}{\Sigma}\int_{-\infty}^{+\infty}\rho\ \sigma_r^2\,{\rm d}z - \langle v_{\rm LOS}\rangle^2\,, \tag{B7}$$

where

$$\Sigma = \int_{-\infty}^{+\infty}\rho\,{\rm d}z$$

is the projected density, x is directed orthogonal to the projection of the rotation axis into the plane of the sky, z is the distance along the line of sight, and $\langle v_\phi\rangle$, σ_r^2 are calculated at intrinsic coordinates x',y' and z'

$$x' = x$$
$$y' = y\,\cos i + z\,\sin i$$
$$z' = -y\,\sin i + z\,\cos i\,,$$

where z' is the height above the equatorial plane and $R = \sqrt{x'^2 + y'^2}$ is the distance from the rotation axis.

This paper has been typeset from a TEX/LATEX file prepared by the author.